Hybrid SnO2/carbon composites: From foams to films by playing with the reaction conditions

(Article begins on next page)

03 October 2024

UNIVERSITÀ DEGLI STUDI DI TORINO

Hybrid SnO$_2$/carbon composites: from foams to films by playing with the reaction conditions

Mohammed Mastabur Rahman, Federico Cesano*, Fabrizio Bardelli, Domenica Scarano and Adriano Zecchina

Nanostructured Interfaces and Surfaces (NIS), Centre of Excellence and Department of IFM Chemistry, University of Turin, Via P. Giuria 7, I-10125 Torino, Italy

*Corresponding author email: federico.cesano@unito.it

Abstract:

Hybrid oxide/carbon composite foams and films were prepared from furfuryl alcohol polymers (PFA) via SnCl$_2$ Lewis acid-catalyzed polymerization and pyrolysis. Structure, morphology and absorptive properties of the porous composites and films were investigated by means of SEM microscopy, XRD, BET analysis and UV-vis spectroscopy. The role of the catalyst concentration and of the thermal treatments were highlighted for both systems. Results concerning the composite foams and films showed that the quality of SnO$_2$ coating was improved upon prolonged thermal treatment at 500°C. Furthermore, the growth behaviour of the SnO$_2$/C and the electrical conductivities of films are also discussed.

Keywords: Hybrid SnO$_2$/carbon composites, foams, films, Lewis acid-catalyzed polymerization, annealing temperature, SnCl$_2$·2H$_2$O concentration.

1. Introduction

Hybrid oxide/carbon composites are interesting materials for a wide range of applications, including high density capacitors, photoelectric devices, gas sensors and photocatalyst [1-3]. At first, due to their large band gap, SnO_2 based semiconductors have excellent optical and electrical properties, chemical/thermal stability. Then, the advantages of using SnO_2/carbon composites have been shown in increasing the electric efficiency and in moderating the fading capacity of Li storage graphite and CNT-based capacitors [4-6]. From the point of view of the sensing properties, the high sensitivity and selectivity of SnO_2/carbon materials towards a wide range of flammable and toxic gases (CH_4, H_2, C_2H_5OH, CO, H_2S, NO_x, NH_3, etc.), have been demonstrated at lower temperature [2]. The high efficiency has been ascribed to the increasing surface area and to the presence of an absorbing and conducting phase. In addition, SnO_2-based nanomaterials have been extensively studied and may serve as chemical sensors and catalysts for environmental and industrial applications [7-13]. Non-stoichiometric and impurity doped SnO_2 thin films are of widespread interest because of their unique properties. These include: high electrical conductivity, optical transparency over the visible wavelengths and high chemical and thermal stability. These properties make them useful for many applications, such as transparent electrodes in various display devices and solar cells [14, 15]. Composite Sn/C thin film can improve its performance as lithium intercalated anode of lithium ion battery [16].

An easy method to prepare oxide/carbon composites (TiO_2/C, ZnO/C) is based on Lewis acid catalysed polymerization of furfuryl alcohol and on the pyrolysis processes of the so-formed polymer composites [3, 17].

It is well known that the Bronsted/Lewis catalyzed polymerization of FA (organic, inorganic acids, protonic zeolites) [18, 19] leads to the formation of carbon-based materials with high surface area and ordered porosity upon thermal treatment ($\approx$700-900°C) and chemical etching (HF, NaOH) [18, 20]. On the other hand, it has also been demostrated that the Lewis acid catalyst ($ZnCl_2$, Ti isopropoxide) is also giving rise to the oxide phases.

The aim of the present work is to show a new approach based on an easy method to prepare hybrid SnO_2/carbon composites in different forms (composite porous foams and films), whose structure, porosity and optical/conducting properties make them suitable for application in capacitors (foam composites) and gas sensor (films).

2. Experimental

2. 1. Synthesis

All the reagents were of analytical grade and used without any purification.

Two kinds of materials have been prepared: carbon composite foams and films. Following Scheme 1, $SnCl_2 \cdot 2H_2O$ salts, preliminarily dissolved in absolute ethanol, were added to different amounts of furfuryl alcohol (FA) (FA:$SnCl_2 \cdot 2H_2O$, 2:1w/w, 4:1w/w and 8:1w/w, respectively), under continuous stirring at room temperature for 15 minutes to make homogeneous solutions. Then, by rising the temperature at ~ 50°C, the formation of porous polymer foams is occurring very rapidly *(Route 1)*. On the contrary, during the films preparation *(Route 2)*, the $SnCl_2$/furfuryl alcohol solutions have been dropped on a Si wafer, then the temperature increased very slowly up to 50-100°C. The obtained composite materials, placed in a quartz tube, were treated at different

temperatures as follows: i) the temperature was increased up to 250°C under N$_2$ (100 ml/min), ii) subsequently air was dosed at 250°C for 1h and iii) then the temperature was increased up to 400°C, 500°C or 750°C under N$_2$ flow, iv) finally the samples were thermally treated for 5h. Films were prepared in the same way.

2. 2. Characterization

After thermal treatments, the morphology and the structure of all composite foams and films were characterized by SEM (Leica Cambridge Stereoscan 420 instrument equipped with an energy dispersive X-ray detector) and XRD measurements (PANalytical X'Pert PRO diffractometer equipped with a Ni filtered Cu K$_\alpha$ radiation in a standard Bragg–Brentano geometry for the bulk materials and Philips PW3020 diffractometer in parallel beam configuration with a fixed low incidence angle of 1.7°, with grazing incidence angle and a Ni filtered Cu K$_\alpha$ radiation for the film characterization). Quantitative phase calculations and crystallite sizes of the samples were obtained by Rietveld analysis of data and Scherrer equation, respectively [21, 22].

N$_2$ adsorption–desorption experiments have been carried out at 77K (Micromeritics ASAP 2020 instrument) on foam materials synthesized at 500°C, to determine the Brunauer–Emmett–Teller (BET) surface area and micropore volume (*t-plot* method). The pore size distribution was determined using Density Functional Theory (DFT) method (Cylindrical Pores in an Oxide Surface geometry). Before the analysis all the samples were outgassed at 150°C for 12h.

Diffuse reflectance UV–vis spectra have been recorded directly at room temperature on foams and films synthesized at 500°C by means of a UV-Vis-NIR spectrometer equipped with a diffuse reflectance attachment (Varian Cary UV 5000 UV-VIS-NIR).

Electrical conductivity analyses have been carried out by means of four point probe measurements.

3. Results and Discussion:

3.1 Morphology, structure and porosity of the composite foam materials

The SEM morphology of the composite foam materials, obtained from FA:SnCl$_2$, 50%wt (2:1) and then thermally treated at 250°C, 400°C, 500°C and 750°C are shown in Fig. 1a, 1b, 1c, 1d (and insets therein), respectively. The sample obtained after thermal treatment at 250°C under N$_2$ and air flows is constituted of hemispheric craters with diameters in the 5 - 10 μm range, due to vaporized SnCl$_2$ drops (EDX data not shown for the sake of brevity), densely distributed on a rough polymer surface (Fig. 1a). As imaged from the enlarged view of Fig.1a, each drop is made by a complex aggregate of many small droplets, which give rise to irregular hollow structures. From XRD pattern (Fig.1e) the presence of very weak peaks of 2θ ≈ 26.6°, 33.9° and 51.8° is observed, which means that small SnO$_2$ crystallites (about 10 nm in diameter) start to form.

The composite foam material, treated at 400°C, exhibits a quite heterogeneous habit, due to the simultaneous presence of circular shapes, remembering the original SnCl$_2$ particles together with irregular cracks, which allows evidence of the underlying support, mainly constituted by the carbon phase (Fig.1b). By selecting one circular shape at higher magnification (inset in Fig.1b), the occurrence of SnO$_2$ nanoparticle aggregates in the 100-350 nm range can be observed, which means that in this temperature range the occurrence of the prevailing SnO$_2$ phase is singled out, even if the presence of residual chlorine cannot be neglected according to EDX analysis (data not shown for sake of brevity). This is supported by XRD pattern (Fig.1f), where peaks at 2θ ≈ 26.6°, 33.9°, 30.0°,

51.8° and 54.8° are associated with the (110), (101), (200), (211) and (220) SnO_2 crystalline planes [6].

By moving to the composite foam material treated at 500°C (Fig. 1c), a regular carpet-like structure formed by nanocrystal aggregates in the 100-400 nm range is highligthed, whose prevalent composition is due to Sn and O, as revealed by EDX analysis (data not reported for sake of brevity). From XRD pattern (Fig.1g), the typical features of SnO_2 phase are again observed together with the formation of Sn particles, as it comes out from the presence of minor peaks at $2\theta \approx 30.6°$, $32.0°$, $43.9°$ and $44.9°$ corresponding to the (200), (101), (220) and (211) crystalline planes of the Sn metal phase [6].

The sample coming from the thermal treatment at 750°C is constituted of spherical particles with a wide distribution of Sn metal clusters in the 100-1500 nm range, rarely distributed on the surface. In this case the carbon phase is playing a relevant role in affecting the complete disappearance of the SnO_2 phase and the simultaneous occurrence of metal Sn (Fig. 1d) at high temperature [6, 23]. To this regard, the remarkable increasing of the peaks associated to Sn phase and the appearance of a broad feature around $2\theta \approx 22°$-$25°$ (Fig. 1h), associated with turbostratic carbon amorphous phase [24, 25], can be highlighted.

A more quantitative analysis, concerning phases and crystallites sizes comes from Rietveld analysis and Scherrer equation. The relative phases weight fractions and crystallite sizes from XRD analysis of composite foams as a function of the thermal treatment temperature and precursor concentration are reported in Table 1. At 250°C small (~10 nm) crystallites of SnO_2 start to form, whereas, at 400°C only the SnO_2 is present and the cristallite sizes are increasing to 31 nm. Going to 500°C, metallic Sn phase is forming with a 1:3 ratio with respect to the still present SnO_2 phase, and the crystallite sizes are ranging from 51 and 40 nm, respectively. Finally, at 750°C only the metallic Sn is present with cristallites of the order of 71 nm.

On the basis of these results and in order to find out the optimum $SnCl_2$ concentration, in Fig. 2a, 2b, 2c three samples coming from different $FA:SnCl_2$ ratios (2:1 w/w, 4:1 w/w and 8:1 w/w) are compared. It comes that on the sample prepared from $FA/SnCl_2$ 2:1 w/w (Fig. 2a), the most regular structure made of a compact layer can be obtained, which is again supported by XRD data (Fig. 2d, 2e, 2f). SnO_2 phase is present in all samples at 500°C, but with different relative amounts with respect to the Sn phase. In more details, the quantitative analysis of the weight fraction from XRD data shows that by increasing the starting $SnCl_2$ precursor concentration, the Sn metal phase is progressively increased, despite of the SnO_2 one.

At the same time the relative weight between the Sn and SnO_2 is reversed by moving from 2:1w/w to 8:1w/w, or in other words the metallic Sn phase is decreasing while SnO_2 increases. On the contrary, cristallite sizes remain quite constant for all concentrations (~34 ÷ 40 nm for SnO_2 and ~51 ÷ 60 nm for Sn).

The adsorption–desorption isotherms of N_2 at 77K of foam materials treated at 500°C, are shown in Fig. 3a,b,c. All the isotherms of the samples are approaching to a large extent the type-I reference isotherms (IUPAC), which indicates the prevalent microporous character of materials. From this figure, it is evident that the $SnCl_2$ loading is affecting the porosity of the pyrolyzed materials and simultaneously the chance for more N_2 to be adsorbed is increasing. From the BET surface area, it results that on decreasing the $SnCl_2$ content, the surface areas are progressively decreasing. All the surface area values are close to those of C/SnO_2 composites obtained by wet impregnation of activated carbons by Al-Kahtib and al. [6, 26].

In Fig. 3d the pore distributions of the three foam materials, as obtained by DFT analysis is reported. From this plot, it can be concluded that the more concentrated samples (2:1w/w and 4:1w/w) are quite similar, whereas some differences can be observed on the more diluted one (8:1w/w). In particular two main peaks at ~8 Å, 10 Å and 14 Å for (2:1w/w) and (4:1w/w) samples are observed, whereas, for (8:1w/w) one additional peak at ~13 Å is detected, which means that for all samples a common microporosity is in general confirmed, even if for more diluted one a slightly more heterogeneous distribution can be observed.

3.2 Morphology and structure of the films

Similarly to the procedure adopted on foam materials, samples starting from FA:SnCl$_2$ (4:1w/w) ratio, were prepared in the form of films on silicon support. SEM images of SnO$_2$/C films obtained at 400°C and 500°C are compared in Fig. 4a and 4b. In both images the presence of an uniform coverage of spherical aggregates, about ~1μm in size is observed, although particles of samples obtained at 500°C, appear more compact and dense, with higher uniformity with respect to those of samples obtained at 400°C. As a matter of fact from XRD patterns (Fig. 4c, 4d), the sample obtained at 500°C shows peaks at 2θ ≈ 26.6°, 33.9°, 38,0°, 51.8° and 54.8° associated with the (110), (101), (200), (211) and (220) crystalline planes of SnO$_2$ phase only [6], while sample treated at 400°C show the co-presence of a SnO phase and SnO$_2$ in 1:1 relative proportion, as testified by the presence of the main peak at 2θ ≈ 30°, corresponding to the (101) SnO crystalline planes *(see table 2)*. Cristallite sizes are lying in the 14 – 21 nm range for both phases and temperatures.

SEM images of films obtained from different FA:SnCl$_2$ ratios (4:1w/w, 6:1w/w and 8:1w/w) and treated at 500°C, are shown in Fig. 5a, 5b and 5c, respectively. The most regular distribution of crystallites and the higher degree of uniformity can be observed on sample coming from 4:1w/w ratio. Crystalline SnO$_2$/carbon films are also obtained from 6:1w/w and 8:1w/w ratios (Fig. 5b, 5c). From XRD data (Fig.5d, 5e, 5f), SnO$_2$ phase is forming again for all samples, but only samples coming from 4:1w/w (SnCl$_2$) the only SnO$_2$ phase is prevailing. On the other samples (6:1w/w, 8:1w/w), the formation of metallic Sn phase is observed to increase by decreasing the precursor concentration *(see Table 2)*.

This anomalous behaviour with respect to that of the foam material, could be explained by considering the different instrumental set-up. As a matter of fact, as all the XRD analyses on films have been carried out at glancing incident angle, only the external layer composition (SnO$_2$) is prevailing on that of metal Sn, which is expected to be in close contact with the underlying carbon phase. Furthermore, all the obtained quantitative data from films are very close, because of the limited range of composition (FA:SnCl$_2$ 4:1÷8:1 wt) that has been investigated (Table 2).

Again, cristallite sizes remain almost constant for all concentrations in the 18-22 nm range for SnO$_2$ and in the 19-21 nm range for Sn.

3.3 Optical properties of the materials

UV-vis spectra of composite foam materials and films obtained from 500°C, are compared in Fig.6a,b respectively. The adsorption edges of the three composite foam materials, coming from different compositions are very similar, and the value of the absorption edge was about 350 nm (Fig.6a).

The adsorption edges of the three films are also quite similar, even if a slight frequency shift towards high wavelength is observed for more concentrated sample (4:1w/w). In particular for (8:1 w/w), (6:1 w/w), samples Eg ≅ 370÷387 nm, while for (4:1w/w) sample, Eg ≅ 407 nm were

evaluated. In the all cases, the absorption edges for the film samples are more shifted toward visible light wavelengths , with respect to those of foam materials.

3.4 Electric conductivity of the films

Conductivity values lie in the $0.7 \div 2.8 \ 10^{-6}$ S/cm range for all the films. These values are comparable to those reported by Kang et al. [27] for pure SnO_2 phase, annealed at 400°C ($\sim 80 \ 10^{-6}$ S/cm), but much lower than those indicated by Chopra et al. [28] for SnO_2 films (10^{-3}–10^{-2} S/cm).

At constant temperature (500°C), an increasing trend in conductivities is observed with decreasing $SnCl_2$ concentration (see Fig. 7). The higher conductivity is in agreement with the appearance and evolution of the reduced phase, corresponding to metal Sn, as obtained from diffraction refinements (see Table 2). At constant $SnCl_2$ dilution (4:1), conductivity appears to be higher by a factor four for the sample treated at lower temperature (400°C). Quantitative phase analysis for this sample shows a biphasic compound with SnO_2 and SnO about 1:1 in ratio; therefore, the latter phase appears to be responsible for the higher conductivity observed [29].

Conclusions

In conclusion, on the basis of the discussed results it can be inferred that the SnO_2/carbon and Sn/carbon based composites can be prepared by Lewis acid catalyzed polymerization of furfuryl alcohol, while absolute ethanol acts as a suitable dispersion agent for this preparations, upon the progressive temperature increasing. Among all the used quantities of $SnCl_2$, the 33%wt (FA:SnCl$_2$ 2:1w/w) and the 20%wt (FA:SnCl$_2$ 4:1 w/w) are more suitable weight percentages to prepare foam materials and films, respectively. While the thermal treatments at low temperature (500°C) give rise to highly crystalline SnO_2/carbon foams, at higher temperature (750°C) Sn particles are formed on a more ordered carbon phase with the simutaneous disappereance of the SnO_2 phase. A higher conductivity is obtained for samples treated at 400°C, where the coexistance of SnO_2 and SnO phases is occurring, whereas for samples treated at 500°C the conductivity is increasing with the formation of Sn reduced phase.

We believe that the presented synthesis method, which leads to the formation of porous composite foams and films mainly constitited by carbon and SnO_2 phases, can be useful for applications in electric devices for energy capacitors and for gas sensing applications.

References:

[1]   Z. Wang, M.A. Fierke and A. Stein, Journal of the Electrochemical Society, 155 (2008) A658.

[2]   B.Y. Wei, M.C. Hsu, P.G. Su, H.M. Lin, R.J. Wu and H.J. Lai, Sensors and Actuators B-Chemical, 101 (2004) 81.

[3]   F. Cesano, S. Bertarione, A. Damin, G. Agostini, S. Usseglio, J.G. Vitillo, C. Lamberti, G. Spoto, D. Scarano and A. Zecchina, Advanced Materials, 20 (2008) 3342.

[4]   Y. Wang and J.Y. Lee, Electrochemistry Communications, 5 (2003) 292.

[5]   Y.J. Chen, C.L. Zhu, X.Y. Xue, X.L. Shi and M.S. Cao, Applied Physics Letters, 92 (2008).

[6]   X.W. Lou, J.S. Chen, P. Chen and L.A. Archer, Chemistry of Materials, (2009).

[7]   A. Salehi, Sensors and Actuators B-Chemical, 96 (2003) 88.

[8]   C.H. Wang, X.F. Chu and M.M. Wu, Sensors and Actuators B-Chemical, 120 (2007) 508.

[9]   Y. Liu, E. Koep and M.L. Liu, Chemistry of Materials, 17 (2005) 3997.

[10]   A. Maiti, J.A. Rodriguez, M. Law, P. Kung, J.R. McKinney and P.D. Yang, Nano Letters, 3 (2003) 1025.

[11]   P. Hidalgo, R.H.R. Castro, A.C.V. Coelho and D. Gouvea, Chemistry of Materials, 17 (2005) 4149.

[12]   A. Kolmakov, Y.X. Zhang, G.S. Cheng and M. Moskovits, Advanced Materials, 15 (2003) 997.

[13]   Y. Cao, X.T. Zhang, W.S. Yang, H. Du, Y.B. Bai, T.J. Li and J.N. Yao, Chemistry of Materials, 12 (2000) 3445.

[14]   W.A. Badaway, Journal of Electroanalytical Chemistry, 281 (1990) 85.

[15]   C. Geoffroy, G. Campet, F. Menil, J. Portier, J. Salardenne and G. Couturier, Active and Passive Electron. Comp., 14 (1991) 111.

[16]   L.Z. Zhao, S.J. Hu, W.S. Li, L.M. Li and X.H. Hou, Rare Metals, 27 (2008) 507.

[17]   F. Cesano, D. Scarano, S. Bertarione, F. Bonino, A. Damin, S. Bordiga, C. Prestipino, C. Lamberti and A. Zecchina, J. Photochem. Photobiol. A-Chem., 196 (2008) 143.

[18]   Z.X. Ma, T. Kyotani and A. Tomita, Carbon, 40 (2002) 2367.

[19]   S. Bertarione, F. Bonino, F. Cesano, A. Damin, D. Scarano and A. Zecchina, Journal of Physical Chemistry B, 112 (2008) 2580.

[20]   Z.X. Yang, Y.D. Xia and R. Mokaya, J. Am. Chem. Soc., 129 (2007) 1673.

[21]   J.R. Carvajal, Physica B: Cond. Matter., 192 (1993) 55.

[22]   L.S. Birks and H. Friedman, Journal of Applied Physics, 17 (1946) 687.

[23]   J. Read, D. Foster, J. Wolfenstine and W. Behl, Journal of Power Sources, 96 (2001) 277.

[24]   V. Petkov, R.G. DiFrancesco, S.J.L. Billinge, M. Acharya and H.C. Foley, Philos. Mag. B-Phys. Condens. Matter Stat. Mech. Electron. Opt. Magn. Prop., 79 (1999) 1519.

[25]   P.J.F. Harris, A. Burian and S. Duber, Philos. Mag. Lett., 80 (2000) 381.

[26]   M.F. Al-Khatib, S.E. Iyuke, A.B. Mohamad, W.R.W. Daud, A.A.H. Kadhum, A.M. Shariff and M.A. Yarmo, Carbon, 40 (2002) 1929.

[27]   S.Z. Kang, Z.Y. Cui and J. Mu, J. Dispersion Sci. Technol., 28 (2007) 569.

[28]   K.L. Chopra, S. Major and D.K. Pandya, Thin Solid Films, 102 (1983) 1.

[29]   J. Calderer, P. Molinas, J. Sueiras, E. Llobet, X. Vilanova, X. Correig, F. Masana and A. Rodriguez, Microelectron. Reliab., 40 (2000) 807.
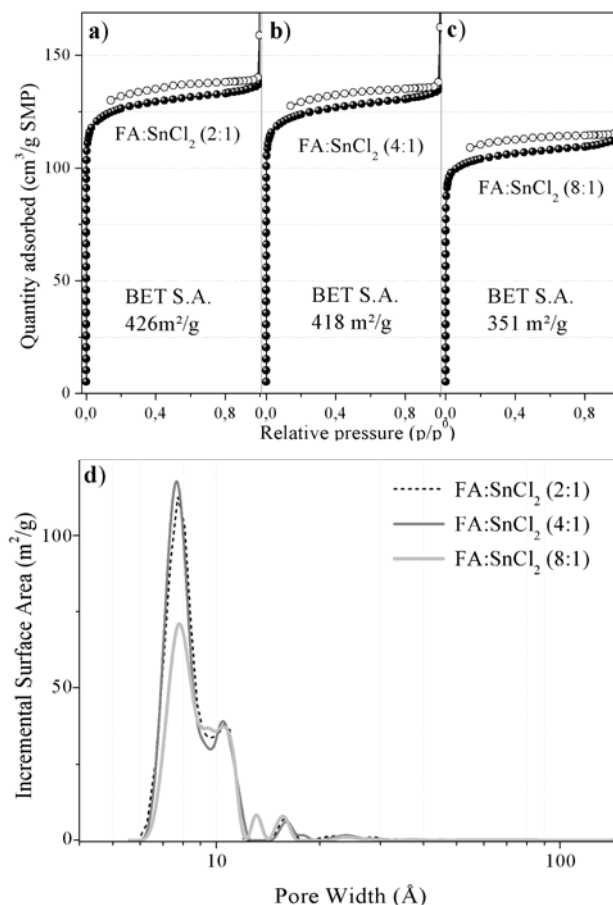
Figures, Figure and Table Captions:
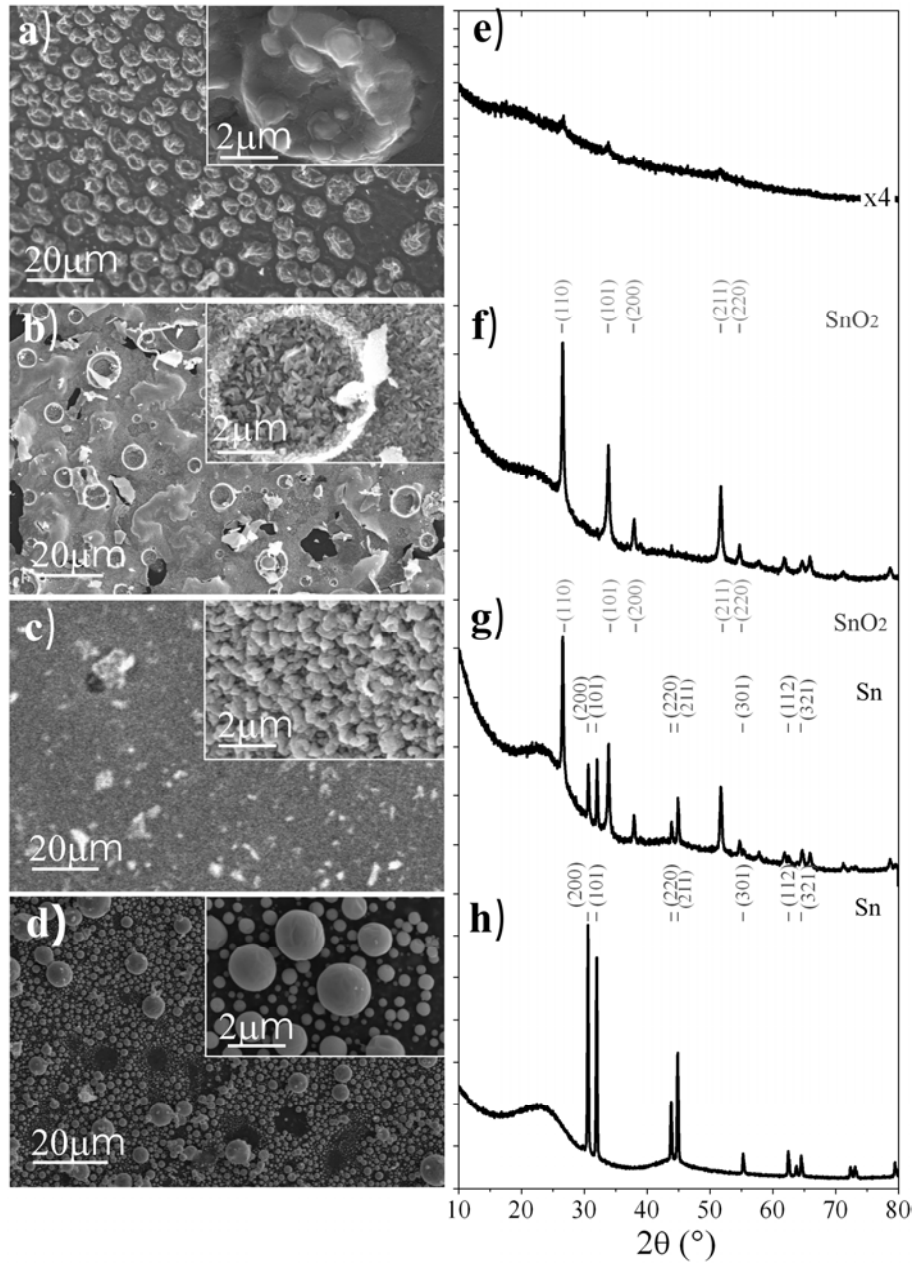
Figure 1. SEM images and XRD patterns of composite foams, treated at $250^{o}C(a,e), 400^{o}C(b,f)$, $500^{o}C(c,g)$ and $750^{o}C(d,h)$, from FA: $SnCl_2$ (2:1 w/w)
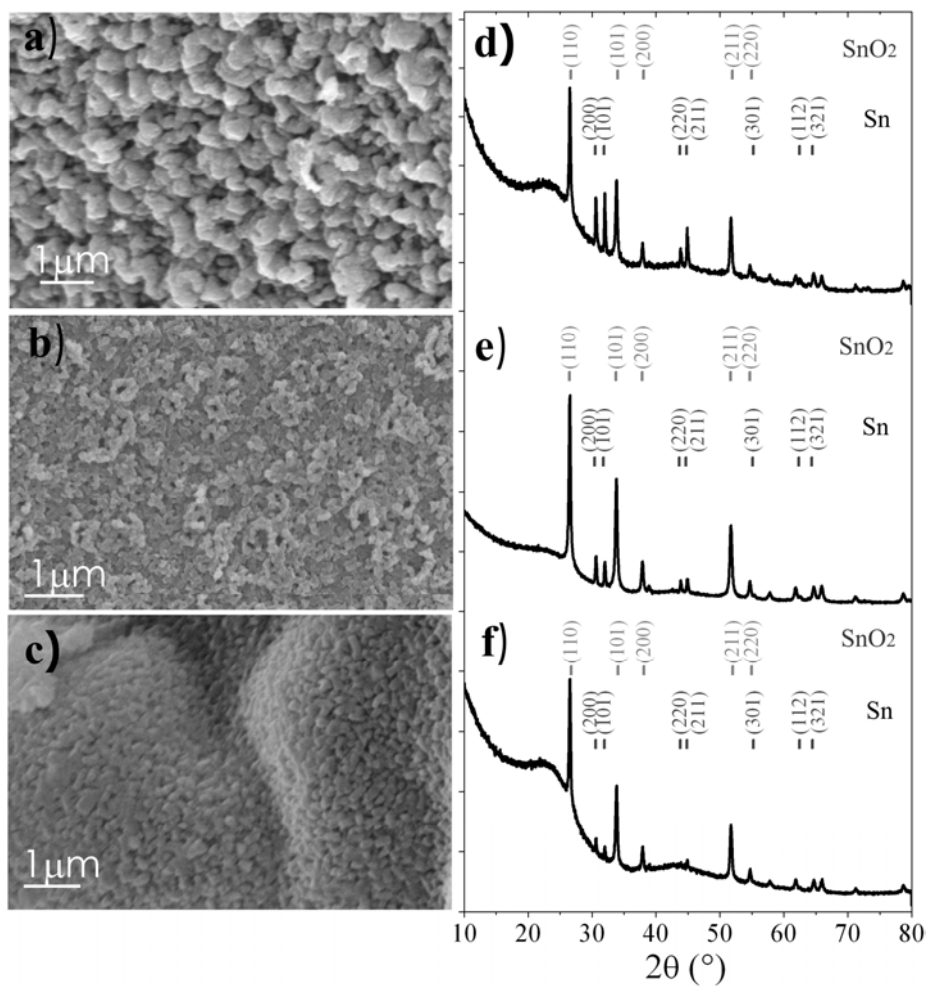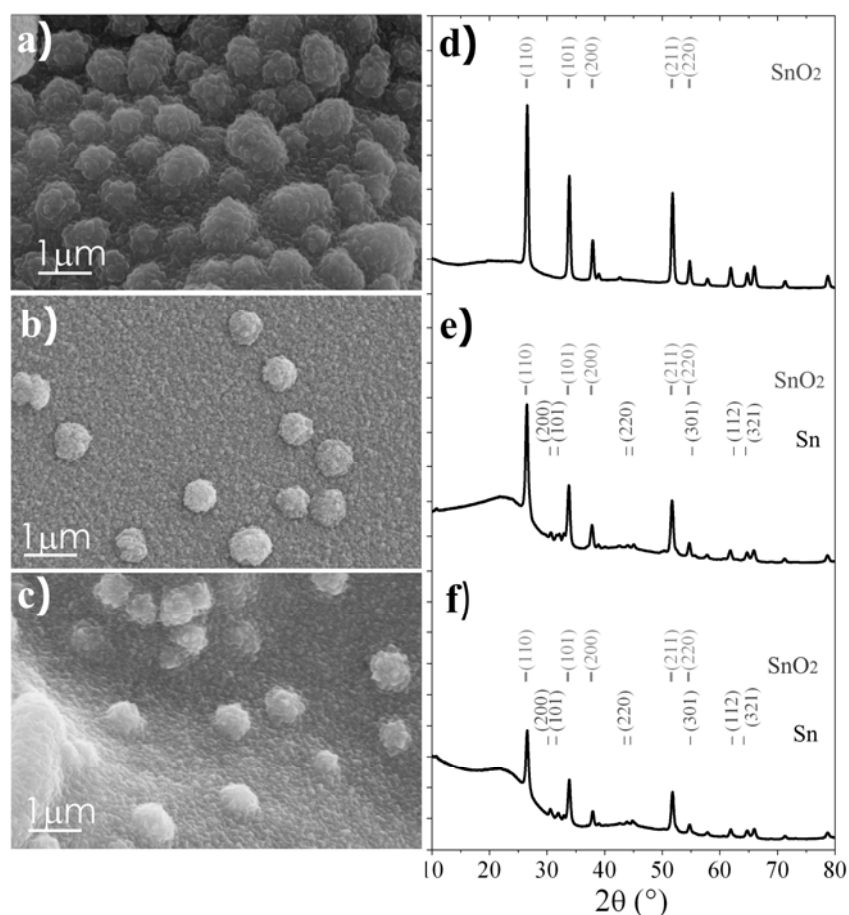
Figure 2. SEM images and XRD patterns of composite foams, treated up to 500°C, obtained from FA:SnCl$_2$(2:1 w/w) (a,d), 4:1 w/w (b,e), and 8:1 w/w (c,f)

Figure 3. N$_2$-adsorption desorption isotherms of composite foams obtained from different percentages of SnCl$_2$ (2:1 w/w, 4:1 w/w and 8:1w/w) and thermally treated up to 500°C for 5h a), b) and c), respectively. Pore size distribution graphs of composite foams, treated up to 500°C, as estimated by DFT method d).
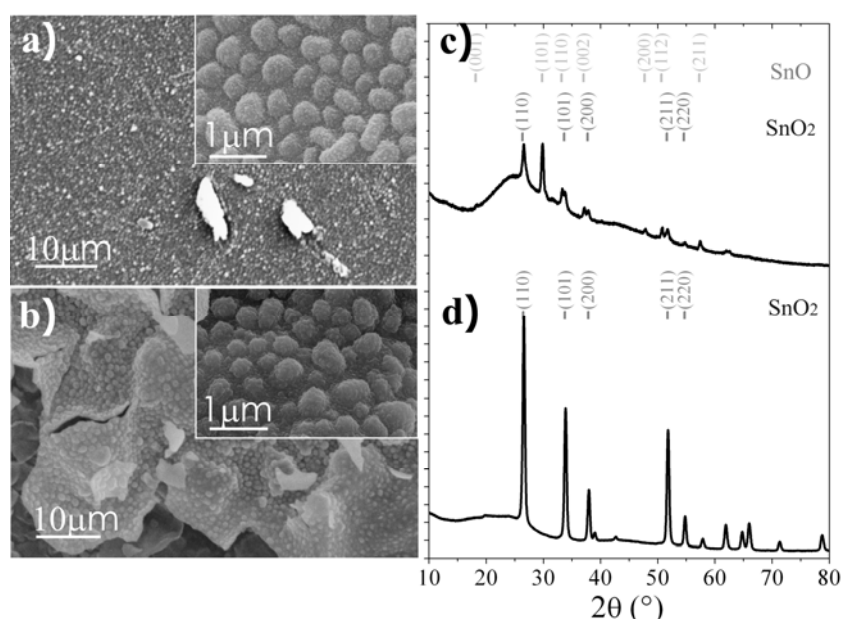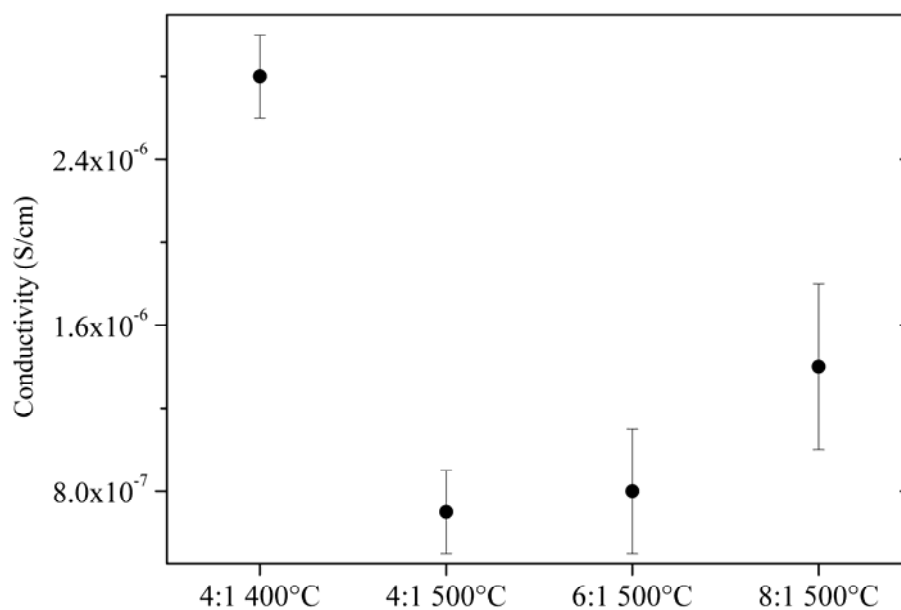

Figure 4. SEM images and XRD patterns of films, treated up to 400°C(a,c) and 500°C (b,d), obtained from FA:SnCl$_2$ (4:1 w/w)

11

Figure 5. SEM images and XRD patterns of films, treated up to 500°C, obtained from FA:SnCl₂, 4:1 w/w (a,d), 6:1 w/w (b,e), and 8:1w/w (c,f).
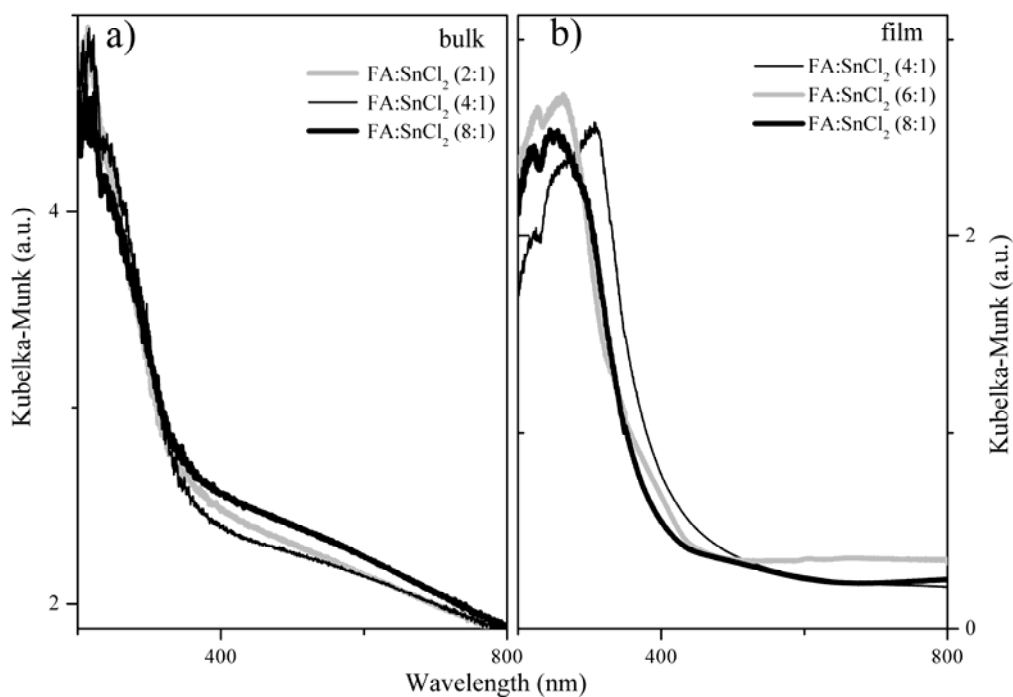
Figure 6. UV-vis spectra of composite foams (a) and films (b) treated up to 500°C

Figure 7. Electric conductivity of films, obtained from different FA and SnCl$_2$ compositions, as treated at 400°C (4:1 %wt) and 500°C (4:1 %wt, 6:1 % wt, 8:1% wt).

2:1	Phases		Crystallite size (nm)
FA:SnCl$_2$ 250°C	SnO$_2$		10(5)
FA:SnCl$_2$ 400°C	SnO$_2$		31(5)
FA:SnCl$_2$ 500°C	Sn	34(1)%	51(5)
	SnO$_2$	66(1)%	40(5)
FA:SnCl$_2$ 750°C	Sn		71(5)
500°C			
FA:SnCl$_2$ 2:1	Sn	34(1)%	51(5)
	SnO$_2$	66(1)%	40(5)
FA:SnCl$_2$ 4:1	Sn	10(1)%	53(5)
	SnO$_2$	90(2)%	34(5)
FA:SnCl$_2$ 8:1	Sn	8(1)%	60(5)
	SnO$_2$	92(2)%	34(5)

Table 1. Relative phases weight fractions and crystallite size from XRD analysis of composite foams treated at 250°C, 400°C, 500°C and 750°C, from FA:SnCl$_2$ 2:1 w/w and of composite foams treated at 500°C from FA:SnCl$_2$ 2:1 w/w, 4:1 w/w, and 8:1 w/w. Number between parentheses represents the error on the last digit.

13

4:1	Phases		Crystallite size (nm)
FA:SnCl$_2$ 400°C	SnO$_2$	51(1)%	15(5)
	SnO	49(1)%	23(5)
FA:SnCl$_2$ 500°C	SnO$_2$		22(5)
500°C			
FA:SnCl$_2$ 4:1	SnO$_2$		22(5)
FA:SnCl$_2$ 6:1	Sn	7(1)%	21(5)
	SnO$_2$	93(2)%	18(9)
FA:SnCl$_2$ 8:1	Sn	12(1)%	19(5)
	SnO$_2$	88(2)%	18(5)

Table 2. Relative phases weight fractions and crystallite size from XRD analysis of films treated at 400°C and 500°C obtained from FA:SnCl$_2$ 4:1 w/w and at 500°C obtained from FA:SnCl$_2$ 4:1 w/w, 6:1 w/w, and 8:1 w/w. Number between parentheses represents the error on the last digit.